Article

Molecular Interactions of a Cu-Based Metal−Organic Framework with a Confined Imidazolium-Based Ionic Liquid: A Combined Density Functional Theory and Experimental Vibrational Spectroscopy Study

Nilesh R. Dhumal,[†] Manish P. Singh,[‡] James A. Anderson,[‡] Johannes Kiefer,[‡,§] and Hyung J. Kim[*,†,∥]

[†]Department of Chemistry, Carnegie Mellon University, Pittsburgh, Pennsylvania 15213, United States
[‡]Materials and Chemical Engineering Group, School of Engineering, University of Aberdeen, Aberdeen AB24 3UE, U.K.
[§]Technische Thermodynamik, Universität Bremen, D-28359 Bremen, Germany
[∥]School of Computational Sciences, Korea Institute for Advanced Study, Seoul 130-722, Korea

ABSTRACT: The interactions between a Cu-based metal−organic framework (MOF), Cu-BTC, and an ionic liquid (IL), 1-ethyl-3-methylimidazolium ethyl sulfate, were studied by employing density functional theory (DFT) calculations and vibrational spectroscopy. The Fourier transform infrared (FTIR) and Raman spectra show that the confinement of the IL in the MOF has significant impact on the structure of the MOF as well as on the IL. Raman spectra and DFT calculations reveal a perturbation of the symmetry of the MOF structure due to the interaction of the IL anion with the Cu ions. FTIR and Raman spectra show that the molecular interactions in turn influence the structure of the ion pair. Inside the MOF, two different types of structure of IL ion pairs are formed. One ion-pair structure exhibits enhanced interionic interactions by strengthening the hydrogen bonding between cation and anion, whereas the other structure corresponds to weaker interactions between the IL cation and anion. Moreover, it is shown that the IL imidazolium ring can directly interact with either the MOF or the anion. The difference electron density analysis by DFT calculations indicates that molecular interactions of MOF and IL are accompanied by a transfer and redistribution of electron density.
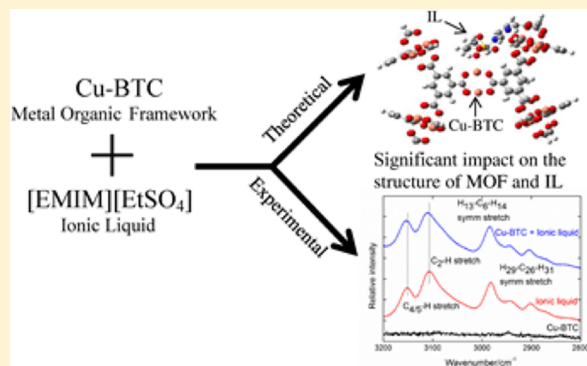
■ INTRODUCTION

Metal−organic frameworks (MOFs) constitute a new generation of porous crystalline materials, which are composed of metals or small clusters of metal sites connected by organic functional groups as linkers. The MOF structure can be tuned to a desired geometry by combining suitable inorganic metals and organic functional groups. MOFs are of great interest because of their exceptionally large surface areas, large pore volume, remarkable storage capacity, and controlled pore textures. They have recently received much attention because of their excellent properties for gas purification, catalysis, molecular sensing, and hydrogen storage.[1−6] Additionally, MOFs are promising materials for the separation of gas mixtures, for example in the field of carbon capture and storage (CCS). Hence, MOFs are a matter of not only scientific curiosity but also potential societal interest in the context of modern energy technology, environmental protection, and global warming.[7]

Room-temperature ionic liquids or simply ionic liquids (ILs) have also gained wide interest because of their unique properties including low melting points, negligible vapor pressure, nonflammability, large electrochemical window, and good thermal and chemical stability, particularly in the presence of air and moisture.[8−14] Due to these unique properties, ILs have demonstrated or proposed applications in a wide range of areas, including many industrially important processes. Example applications can be found in chemical synthesis, catalysis, separation, and extraction as an environmentally benign alternative to organic solvents; energy storage and conversion devices, such as batteries, fuel cells, supercapacitors, and solar cells, as an efficient alternative to conventional electrolytes; and development of novel materials for engineering applications.[15−19] Ionic liquids offer high ionic conductivity and are especially resistant to oxidation, which explains the extensive electrochemical studies in which they are the focus.[20] Recently, the use of ionic liquids to replace organic solvents in biocatalytic processes has also received much attention.[21,22]

Confinement of ILs in the micropores of MOFs may result in tunable hybrid materials, which can increase the number of applications of confined IL systems.[23] Such a tunable hybrid

material is different from previously studied IL-confined systems[23] in a way that an opportunity exists to modify either or both the MOF (host) and the IL (guest) in a very flexible manner. The properties of the MOF can be tuned by varying the structure type, organic functionality, geometry and size of the metal-containing unit, and the size of the pores and of the nanocrystals. The IL provides further flexibility in this hybrid material because of its tunability by changing cations and anions to meet the needs of any specific application. Consequently, the tunable hybrid material based on an IL confined in a MOF could open the possibilities of new applications in, e.g., high-performance electrochemical energy storage and conversion devices including batteries and supercapacitors. For example, the performance of electrical double-layer capacitors (EDLCs) is currently limited by several factors: the specific surface area, the match of the electrode pore structure and the electrolyte, and the double-layer (film) thickness. ILs have the potential to replace the conventional (aqueous and organic) electrolytes because of their many desirable features, and MOFs can provide further flexibility to tailor the surface area, pore size and geometry, size of the metal-containing unit, organic functionality, etc. Therefore, the performance of EDLCs can be improved by the optimization of the pore size, the electrode, and the electrolyte, which is possible by using ILs confined in MOFs. IL/MOF hybrid materials may provide an alternative to current material combinations used in EDLCs.

Surprisingly, there has been only one experimental study investigating the confinement of an IL (1-ethyl-3-methyl-imidazolium bis(trifluoromethylsulfonyl)imide) in a MOF (ZIF-8 or 2-methylimidazole zinc salt) to our knowledge.[24] Once confined inside the MOF, no freezing transition of the IL was observed down to 123 K even though the freezing temperature of the bulk IL is 231 K.[24] On the theory side, only a limited number of computational studies of ILs confined in MOFs have been reported.[25−28] Calero and co-workers studied CO_2 gas adsorption in IL/MOF systems based on copper benzene-1-3-5-tricarboxylate (Cu-BTC) using molecular dynamics (MD) and Monte Carlo (MC) simulations.[25] Jiang and co-workers examined similar IL effects in Zn-based IRMOF.[26] These simulation studies suggest that combinations of an IL and a MOF could provide a promising composite material for CO_2 capture. However, the results of classical simulations need to be interpreted with care. The anions of the IL can couple strongly with the MOF metal centers. This can result in structural modifications. Using a dissociable force-field description,[29] Abroshan and Kim[28] showed that rigid or nondissociable MOF potential models, which are often employed in classical simulations, failed to detect important structural changes of the MOF induced by the confined IL.

The present study aims at making a step-change in the understanding of how imidazolium ILs behave at the molecular level upon confinement in a MOF. For this purpose, a combination of theoretical and experimental approaches has been employed. Ab initio calculations were used to identify possible interacting sites and structural changes due to interactions between the IL and the MOF, when one ion pair is confined per unit pore. Fourier transform infrared (FTIR) and Raman spectroscopy were employed to study the IL/MOF system experimentally. An analysis of the molecular electrostatic potentials (MESP) was performed to find the possible binding sites of the IL inside the MOF. As a model system, the combination of the IL 1-ethyl-3-methylimidazoium ethyl sulfate

(EMIM-ETS) and the MOF copper benzene-1-3-5-tricarboxylate (Cu-BTC) has been chosen. Both materials are commonly used and have been characterized extensively.[30−48]

The outline of this paper is as follows: a brief description of computational and experimental methods used in our study is followed by a detailed analysis of computational and experimental results for IL−MOF interactions and their influence on structures of both the IL and MOF. Concluding remarks are offered at the end.

■ COMPUTATIONAL METHODS

The Cu-BTC MOF consists of Cu as the metal center and BTC as the organic linker. The model system employed in the present study, which is based on the crystal structure geometry, is displayed in Figure 1. Cu-BTC is formed by two big central pores, the larger of which is 9 Å in diameter, and the smaller is 5 Å in diameter.[27]
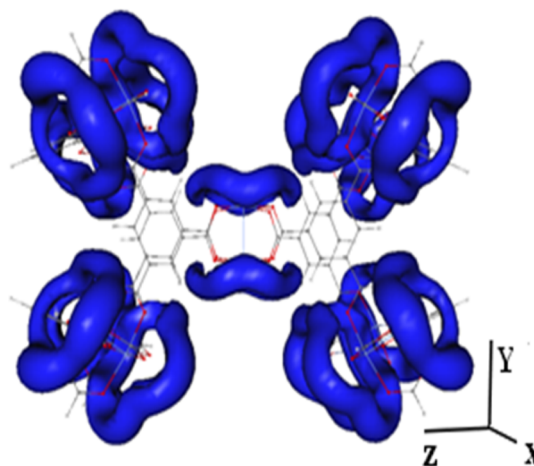

Figure 1. MESP isosurfaces ($V = -52.51$ kJ mol^{-1}) of Cu-BTC model.

By employing a hybrid density functional theory incorporating Becke's three-parameter exchange with Lee, Yang, and Parr's (B3LYP) correlation functional,[49,50] we performed ab initio calculations for the Cu-BTC model MOF system (Figure 2). The MOF system containing one pair of EMIM and ETS
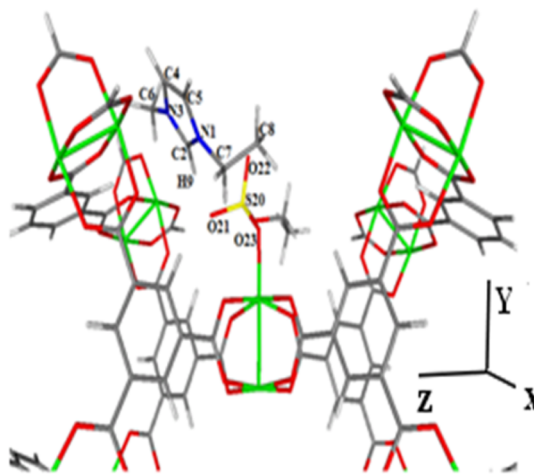

Figure 2. B3LYP/6-31G(d,p) optimized MOF−ion-pair geometry (red, oxygen; white, hydrogen; gray, carbon; green, copper; yellow, sulfur; blue, nitrogen).

ions was also studied. The internally stored 6-31G(d, p) basis set using the Gaussian 09 program[51] was used. In the case of the MOF–IL system, an IL ion pair was initially placed in the larger pore of Cu-BTC in such a way that the ETS anion can interact with a Cu atom of MOF while the repulsion between the anion and MOF oxygen atoms is minimized. The geometry of the lowest-energy conformer reported previously[42] was used for the insertion of the EMIM-ETS ion pair. Once the ion pair was placed inside the MOF, the geometry of the entire MOF–ion-pair system was optimized with B3LYP/6-31G(d, p). We used the default criteria for convergence of the ab initio calculations and the geometry optimizations in the Gaussian 09 program.[51]

The molecular electrostatic potential (MESP)[52] of the pure MOF

$$V(\mathbf{r}) = \sum_{A=1}^{N} \frac{Z_A}{|\mathbf{r}-\mathbf{R}_A|} - \int \frac{\rho(\mathbf{r}')\,d^3\mathbf{r}'}{|\mathbf{r}-\mathbf{r}'|} \tag{1}$$

was calculated, where Z_A and $\mathbf{R}_A$ are the charge and position of nucleus A, respectively; the sum is over all nuclei of the system, and $\rho(\mathbf{r})$ is the electron density. $V(\mathbf{r})$ comprises the bare nuclear potential and the electronic contributions and thus sheds light on the effective localization of electron-rich regions in the molecular system. Therefore, the MESP can be used to determine possible binding sites for the IL inside the MOF. The MESP isosurface was plotted using the UNIVIS-2000 code.[53] The difference electron density $\Delta\rho = \rho_{MOF+IL} - (\rho_{MOF} + \rho_{IL})$ was also computed to investigate the electron density redistribution induced by the MOF–IL interactions. Here, ρ_{MOF+IL} is the electron density of the combined MOF–ion-pair system, while ρ_{MOF} and ρ_{IL} denote those of the isolated MOF and ion-pair complex, respectively.

■ EXPERIMENTAL METHODS

Chemicals. 1-Ethyl-3-methylimidazolium ethyl sulfate was purchased from Alfa Aesar (99%) and used as received. The Basolite C300 (also known as HKUST-1 or Cu-BTC) was purchased from Sigma-Aldrich. Both chemicals are highly water sensitive; hence, care was taken in handling to avoid contact with ambient humidity.

Infrared Spectroscopy. The FTIR spectrum was recorded from 4000 to 500 cm^{-1} on an attenuated total reflection (ATR) module with a Bruker Vertex 70 instrument at 0.5 cm^{-1} nominal resolution. The number of reflections at the diamond crystal surface was 1. For the measurement of the IL, a droplet was placed on the ATR crystal and covered with a glass cap to avoid absorption of moisture from the surrounding air. For the measurements of the Cu-BTC containing samples, a moderate pressure was applied on the samples to achieve optimal contact between the solid sample and the ATR crystal. Sixteen scans were averaged to obtain appropriate signal-to-noise ratio. All spectra were background corrected for water and CO$_2$.

Raman Spectroscopy. Raman spectra were recorded from 4000 to 100 cm^{-1} with a spectral resolution of 1 cm^{-1} using a Renishaw inViaRaman microscope (Renishaw Plc, Gloucestershire, UK) fitted with a 514 nm Argon ion laser and using a grating of 2400 lines/mm. The exposure time was 10 s, and 100 spectra were accumulated per run. The collection optics was set at 50× objective. To avoid decomposition of the sample, the laser power was limited to the setting of 5% (100% power = 15 mW at the sample).

All FTIR and Raman spectra were normalized with respect to their individual maximum absorbance/intensity.

Sample Preparation. IL-impregnated Cu-BTC samples were prepared by mixing x = 38.6 wt % (61.4 mol %) IL and Cu-BTC. This stoichiometry means that the ratio of ion pairs and Cu-BTU pores is approximately 0.81. Subsequently, the samples were heated at 60 °C for 24 h to obtain a homogeneous distribution of IL in the pores of the Cu-BTC. This ensured that the majority of MOF pores contained one IL ion pair representing the situation in the simulation. We note that a small amount of adsorbed water was present in the samples. Water adsorption in Cu-BTC can lead to a degradation of the material,[54] but these processes take place on a time-scale significantly longer (days and weeks) than the experiments reported here (minutes and hours). Indeed, changes of the samples with time were not observed in our study. The presence of adsorbed water was taken into account in the analysis and discussion of the experimental results to make contact with the computational results. Water molecules were not included in the latter because the main purpose of the present work is to investigate the interactions between the MOF and IL and their influence on the respective structures of the MOF and IL.

■ RESULTS AND DISCUSSION

To unravel the interactions between the ionic liquid and the metal–organic framework, a three-step analysis is performed. First, possible interaction sites are identified and the impact of the presence of the IL on the MOF structure is studied. In the second step, the situation from the IL perspective focusing on the MOF's impact on the IL pair is studied. The third step brings both aspects together to obtain an integrated picture of the overall phenomena.

MOFs have large surface areas with controlled pore textures. To find the most likely binding site for the ionic liquid to interact with the MOF, it would be interesting to understand the localization of electron density within the MOF structure. MESP reveals the effective localization of the electron-rich regions within the molecular system. The MESP isosurfaces (V = −52.51 kJ mol^{-1}) of the model Cu-BTC MOF system are depicted in Figure 1. Overall, the electron density is distributed symmetrically within the MOF structure, but it is more delocalized around the oxygen atoms of the linker molecules. When an ion pair of the ionic liquid is placed inside a pore of the MOF, different types of molecular interactions can take place. For example, the hydrogen atoms of the cation can have an electrostatic interaction with the oxygen atoms of the linkers. The electronegative atoms of the anion, i.e., oxygen atoms, can interact with the MOF metal ions or with the IL cation. We proceed to the computational and experimental data to obtain detailed information on the nature of the IL–MOF interactions at the molecular level and understand the consequences of these interactions.

Effects on MOF Structure upon Confinement of IL. In view of the potential impact of the IL on the MOF structure,[28] analysis of their interactions was performed by comparing the geometry of the pure EMIM-ETS, pure MOF, and the combined system of MOF with IL confined inside. The DFT result for the optimized MOF–ion-pair conformation is shown in Figure 2, while those for selected geometrical parameters of the isolated ion pair and the pure Cu-BTC, as well as the Cu-BTC–ion-pair system are compiled in Table 1. The experimental FTIR and Raman spectra of the pure IL, MOF,

Table 1. Selected Geometrical Parameters of Pure Ionic Liquid, Cu-MOF Model, and Ion-Pair−Cu-MOF Model

parameters[a]	IL	MOF	ion-pair−MOF
d(Cu−Cu)		2.525	2.632
d(Cu−O) inside the pore		1.973	2.001,2.035,1.996,2.016
			1.970[b],1.977[b],1.968[b],1.973[b]
d(C−O) inside		1.272	1.266,1.266,1.266,1.264
			1.272[b],1.273[b],1.274[b],1.271[b]
d(Cu−O$_{anion}$)			2.140
d(C2−H)	1.088		1.095
d(C2−H···O)	1.920,2.183		1.880
d(SO)	1.467$_{free}$, 1.496, 1.491, 1.666		1.477, 1.484$_{cation}$, 1.505$_{MOF}$, 1.634
a(O−Cu−O)		90	88.6, 90.2, 87.7, 88.3
			88.57, 91.52, 80.04, 90.6
a(O−Cu−O) opposite		172	162.5[b], 162.5[b]
			176.2, 176.0

[a]d, distance; a, angle. [b]Bond participating in the interaction with IL.

and their mixtures are displayed in panels A and B of Figure 3, respectively, and the vibrational frequencies are summarized in Table 2. Spectra a, b, and c in Figure 3 are the results for 38.6 mol % Cu-BTC with IL, pure IL, and pure Cu-BTC, respectively. The assignments are based on work reported in the literature for the IL[41] and the MOF.[39,54−56] According to
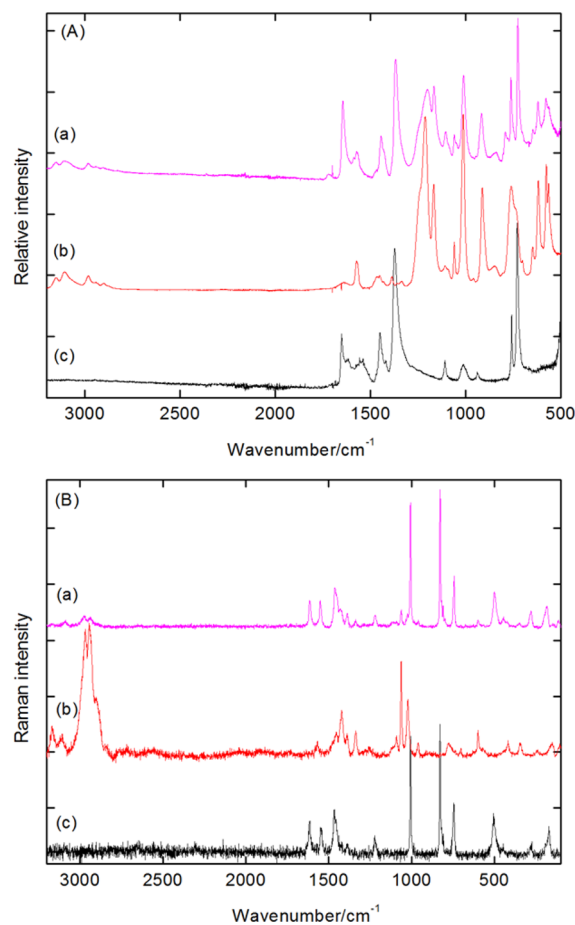

Figure 3. Experimental (A) FTIR and (B) Raman spectra: (a) 38.6 mol % Cu-BTC with IL, (b) pure IL, and (c) pure Cu-BTC.

the DFT analysis, the interaction between the oxygen atom of the anion and the MOF Cu ion results in the elongation of the Cu−Cu bond by 0.107 Å with respect to 2.525 Å in the pure MOF. The Cu−O distances of the MOF in the metal center region where the oxygen atoms of the MOF linker molecules bind to Cu atoms are also elongated when Cu interacts with the anion. By contrast, the Cu−O distances for the Cu ions not interacting with the anion are generally shortened. The angle of O−Cu−O (oxygen in opposite position) is reduced by approximately 10° from 172° to ~162° for Cu interacting with the IL anion. Thus, the interaction with the IL anion pulls the Cu ion away from the four carboxylate oxygen atoms that coordinate Cu. By contrast, Cu not interacting with the anion becomes slightly more coplanar with its four coordinated oxygen atoms. Considering that the change in molecular geometry generally depends on the strength of the interaction, the O−Cu−O angle change of 10° seems to suggest that the interaction between the MOF and IL is not weak. Our findings here via DFT indicate that introduction of IL into the MOF disturbs the highly symmetric MOF structure.

The interaction between the IL and the MOF also manifests in the experimental vibrational spectra. The bands associated with the Cu ions in the MOF appear in the spectral range below 600 cm^{-1}. This part of the Raman spectrum is shown enlarged in Figure 4. In the pure MOF (spectrum c of Figure 4), two bands at 505 (strong) and 449 cm^{-1} (weak) and a doublet in the 193−172 cm^{-1} range are attributed to Cu−O and Cu−Cu stretching modes, respectively. The presence of the doublet for the latter assignment indicates that the MOF is partly hydrated,[39] which is also suggested by the feature at 281 cm^{-1} as this band would not appear in the completely dehydrated MOF. The bands are shifted when the IL is impregnated into Cu-BTC (spectrum a of Figure 4). The doublet at 193 and 172 cm^{-1} were shifted to 205 and 185 cm^{-1}, respectively. The Cu−Cu bond elongation predicted in the computational data would predict a decrease in the frequency of the corresponding stretching modes, while the Raman spectrum indicated that the particular mode is blue-shifted. This seems to be a contradiction at first glance. However, it should be borne in mind that the MOF is partly hydrated. The outgassed MOF would show a Cu−Cu band at 228 cm^{-1}.[39] With respect to this value, the Raman data actually show a decrease in the frequency as predicted in the simulation. The bands at 505 and 449 cm^{-1} are slightly shifted to 502 and 446 cm^{-1}, respectively. Those bands are likely to originate from Cu−O vibrations, and a decrease in the frequency suggests a weakening of the bond, which is in concert with the bond elongation observed in the simulation. This indicates that the modes involve Cu interacting with anions. The Cu−O bond, in which the Cu is not involved in the interactions, would show an increase in frequency upon bond shortening. This is not observed.

The spectral range from 1700 to 1200 cm^{-1} is dominated by characteristic modes of the MOF linker molecules as can be seen in the FTIR and Raman spectra displayed in panels A and B of Figure 5, respectively. FTIR features are observed at 1652, 1450, 1419, and 1374 cm^{-1} in the pure Cu-BTC. All these bands are assigned to vibrations of the carboxylate group of Cu-BTC. The presence of four bands suggests the existence of two different types of carboxylates in the MOF exhibiting one pair of asymmetric and symmetric COO stretching modes each. The first pair of asymmetric ν_{as}(COO) and symmetric

Table 2. Experimental Raman/IR Vibrational Frequencies (cm^{-1}) of Pure and Confined System

EMIM-ETS Raman/IR	Cu-BTC Raman/IR	EMIM-ETS−Cu-BTC (38.6 mol %) Raman/IR	assignments	EMIM-ETS Raman/IR	Cu-BTC Raman/IR	EMIM-ETS−Cu-BTC (38.6 mol %) Raman/IR	assignments
3169/3151	−/−	−/3152	$C_{4/5}$−H stretch	−/1169	−/−	−/1169	N_1−C_2−H_2 + O_{21}−S_{20}−O_{22} asym stretch
3111/3106	−/−	−/3109	C_2−H stretch	−/1108	−/−	−/−	H_{29}−C_{26}−H_{30} twist
−/−	−/−	3089/3084	C_2−H stretch	−/−	−/1112	−/1105	C−H in plan bending of ring (MOF)
−/2982	−/−	2982/−	symm H_{13}−C_6−H_{14} stretch	1091/1091	−/−	−/−	H_{13}−C_6−H_{14} twist
2968/−	−/−	2975/−	C−H stretching vibration of isolated anion	1063/1060	−/−	1063/1060	O_{24}−C_{25} stretch
2943/−	−/−	2937/−	symm H_{27}−C_{25}−H_{28} stretch	1023/1013	−/1013	1025/1011	C_2−N_1−C_5 stretch/C−H stretch (MOF)
−/2941, 2901	−/−	−/−	symm H_{29}−C_{26}−H_{31} stretch	−/−	1008/−	1006/−	symm stretch (C=C) benzene ring (MOF)
−/−	−/1652	−/1645,−	asymm stretch (COO) (MOF)	−/−	−/−	972/−	−
−/−	1616,1547/−	1614, 1552/−	symm stretch (C=C) benzene ring (MOF)	961/−	−/−	959/−	O_{21}−S_{20}−O_{22} symm stretch
	/1617,1545	−/−	H_2O bending	−/−	−/939	−/−	O−H bending (MOF)
−/−	−/−	−/1588	−	−/913	−/−	−/917	O_{21}−S_{20}−O_{22} symm stretch
1571/1571	−/−	−/1571	N_3−C_4−H_{10} rock	−/−	828/−	−/−	C−H out-of-plane bending of ring (MOF)
−/−	1467/1450,	1462/1444,	asymm stretch (COO) (MOF)	−/807	−/−	−/−	N_1−C_2−H_9 wag
1454/−	−/−	−/−	H_{15}−C_7−H_{16}, H_{18}−C_8−H_{19} scissor	−/−	−/−	811/−	−
1422/1431	−/−	1427/	H_{12}−C_6−H_{13} rock	777/−	−/−	−/−	$H_{15}C_7H_{16}$ wag
−/−	−/1419	−/−	symm stretch (COO) (MOF)	−/761,702	−/759,−	−/762,−	S−O stretching (IL), C−H out-of-plane bending of ring (MOF)
1389/1387	−/−	1388/−	H_{15}−C_7−H_{16}, H_{18}−C_8−H_{19} rock	−/734	746/729	745/727	S_{20}−O_{24} stretch (IL), C−H out-of-plane bending of ring (MOF)
−/−	1388/1374	1388/1368	symm stretch (COO) (MOF)	−/648	−/−	−/647	CN bonding oscillation
−/1335	−/−	−/−	N_1−C_7−H_{16} rock	599/618	−/−	−/620	N_1−C_7 stretch
−/−	1338/−	1339/	H_{15}−C_7−H_{16} rock	−/577	−/−	/579	O_{21}−S_{20}−O_{22} wag
−/−	1271/−	−/−	−	−/−	505/−	502/−	Cu(II) species (MOF)
−/1243	1241/−	−/−	N_1−C_2−H_9 rock + S_{20}−O_{23} stretch	−/−	449/−	446/−	Cu(II) species (MOF)
−/−	1222/−	1220/−	−	420,345/−	−/−	−/−	O_{21}−S_{20}−O_{22} bend
−/1213	−/−	−/1201	S_{20}−O_{23} stretch	−/−	276/−	281/−	Cu(II) species (MOF)
−/−	−/1187	−/−	−	−/−	193/−	205/−	Cu(II) species (MOF)
				−/−	172/−	185/−	Cu(II) species (MOF)

stretching ν_s(COO) vibrations are the bands at 1652 and 1419 cm^{-1}, respectively.

These modes can be assigned to those carboxylate groups located in the big pores of Cu-BTC. This assignment is supported by additional FTIR spectra (not shown) recorded in MOF samples with systematically varied water content. Water can penetrate only the large pores, where it protonates the carboxylate groups. Hence, the intensity of the 1652 and 1419 cm^{-1} bands decrease and at the same time, signals around 1700 and 1200 cm^{-1} characteristic of carboxylic acid groups appear. On the other hand, the bands at 1450 and 1374 cm^{-1} can be assigned to asymmetric and symmetric stretching vibrations of those carboxylate groups located in the smaller pores. Water cannot penetrate in significant amounts; hence, the bands slowly develop minor changes upon water addition (not shown). These findings are in agreement with the observations of DeCoste et al.[54] Other Cu-BTC bands in this spectral region are found at 1617 and 1545 cm^{-1}. They can be assigned to the

bending mode of molecular water. The broad band at 1545 cm^{-1} is due to water coordinated with Cu in the MOF.

Upon confinement of the IL in Cu-BTC, all four carboxylate modes in the FTIR spectrum shift toward lower frequency. Interestingly, the absorbance of those bands assigned to groups in the large pores is enhanced relative to those in the small pores. The peak at 1652 cm^{-1} is shifted to 1645 cm^{-1}, whereas the symmetric stretching vibration is identified as a broad shoulder peak and the exact position is difficult to quantify. Notable shifts to lower frequencies are also observed for the second pair of modes from 1450/1374 to 1444/1368 cm^{-1}. The shifts of both mode pairs of the carboxylate groups indicate an elongation of the associated bonds. In other words, the intermolecular interactions between the linker molecules and the copper become weaker upon interaction with the IL.

The Raman spectra of the pure and the confined materials give further insights into the interactions between the IL and the MOF. The Raman peaks at 1616 and 1547 cm^{-1} in the
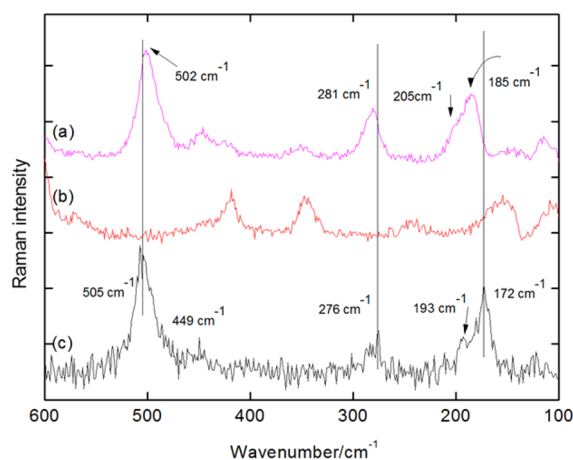
Figure 4. Experimental Raman spectra in the region of 600−100 cm^{-1}, which is characteristic of vibrational bands associated with the MOF Cu ions: (a) Cu-BTC with IL, (b) pure IL, and (c) pure Cu-BTC.
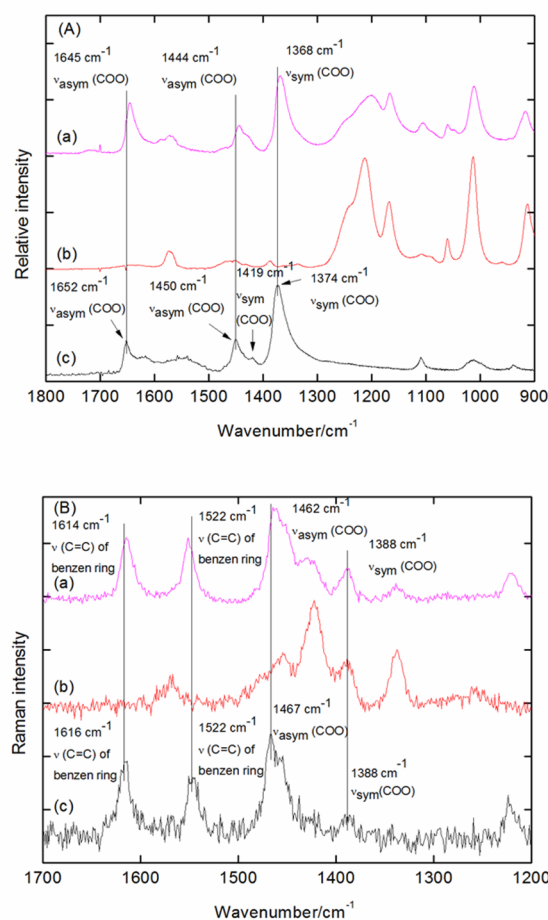

Figure 5. Experimental (A) FTIR and (B) Raman spectra in the range from 900 to 1800 cm^{-1} and 1200−1700 cm^{-1}: (a) Cu-BTC with IL, (b) pure IL, and (c) pure Cu-BTC.

MOF spectrum can be assigned to C=C stretching modes of the aromatic rings in the Cu-BTC linker molecules. Upon IL confinement, they remain almost constant as the benzene rings are not directly involved in the main molecular interactions. The 1616 cm^{-1} band is observed at 1614 cm^{-1}, and the 1547

cm^{-1} peak shows an increase in the frequency to 1552 cm^{-1}. This apparent change in frequency is a result of the peak merging with the IL peak at 1571 cm^{-1}. The Raman modes at 1467 and 1388 cm^{-1} are assigned to the asymmetric ν_{as}(COO) and symmetric stretching ν_s(COO) vibrations of carboxylate groups corresponding to the IR modes at 1450 and 1374 cm^{-1}. The band at 1388 cm^{-1} overlaps with a strong IL peak; hence, a change upon IL addition cannot be observed clearly. On the other hand, the 1467 cm^{-1} Raman peak shifts to 1462 cm^{-1}, which is in agreement with the FTIR data. The 1650 and 1419 cm^{-1} vibrational modes in the FTIR spectrum are not visible in the Raman spectrum. These modes may be very weak or Raman inactive.

Effects on IL Structure upon Confinement in MOF. Placing the IL inside the MOF not only leads to conformational changes within the MOF structure but also affects the IL structure. Consequently, this section investigates how the molecular interactions influence the structure of an ion pair inside a MOF pore. In the case of the EMIM cation, the hydrogen atom H$_9$ at the C$_2$ position of the imidazolium ring is one of the main sites for molecular interactions through the formation of hydrogen bonds (Figure 2). According to a previous study, a stable EMIM-ETS ion pair shows complicated interionic interactions of H$_9$ by forming bifurcated hydrogen bonds.[42] In the presence of other molecules, these hydrogen bonds can be either completely replaced by hydrogen bonds to a third species (e.g., to water and alcohols[47]) or weakened if the third species is a weak hydrogen bond acceptor so that it will influence interionic hydrogen bonds, in particular, their strength indirectly.[46] Hence, the C$_2$−H$_9$ bond can serve as an excellent reporter to probe the interionic and intermolecular interactions.

The DFT results for the changes in the geometry of the IL ion pair upon confinement within Cu-BTC are summarized in Table 1. We notice that the C$_2$−H bond distance is elongated by 0.007 Å while the C$_2$−H$_9$···O$_{21}$ distance decreases by 0.04 Å in the MOF. Both changes suggest a significantly strengthened interionic interaction via hydrogen bonding. The corresponding C$_2$−H$_9$ stretching mode is found at 3106 cm^{-1} in the FTIR spectrum (Figure 6A). The peak appears to shift slightly toward higher frequency to 3109 cm^{-1}, implying a contraction of the C$_2$−H$_9$ bond and the weakening of the interionic hydrogen bond. At first glance, this would suggest disagreement between the computational and the experimental results. However, closer inspection of the spectrum clearly reveals a new shoulder at around 3084 cm^{-1} in the confined sample. This significantly perturbed contribution is most likely due to ion pairs inside the MOF pores. It is possible that not all of the IL finds its way to the interior of the MOF during sample preparation; hence, a contribution from residual bulk liquid may be responsible for the band at 3109 cm^{-1}. To verify this hypothesis, further experiments were conducted with different MOF/IL ratios to change the ratio of confined IL to bulk IL. The data (not shown) corroborate the above interpretation. The appearance of the shoulder band at 3084 cm^{-1} in the FTIR spectrum is further supported by the Raman spectrum, in which the presence of an analogue band is observed at 3089 cm^{-1}, while the C$_2$−H peak of the pure IL is located at 3111 cm^{-1}. Interestingly, the new band is quite strong when comparing the relative intensities in the Raman spectra. This indicates that the influence of the MOF also changes the polarizability of the C$_2$−H bond. In summary, the computational and experimental data suggest that the confinement of ion pairs in the pores of the
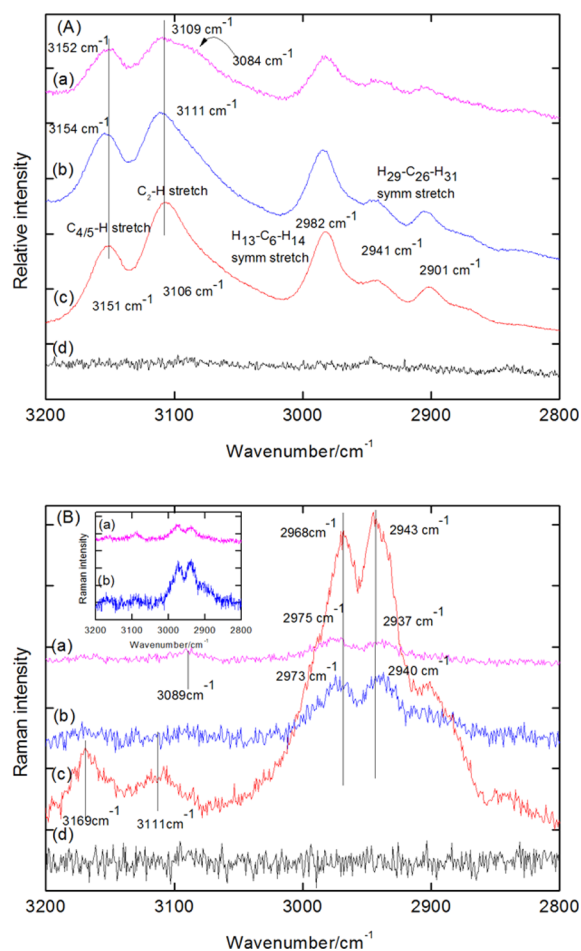
Figure 6. Experimental (A) FTIR and (B) Raman spectra: (a) 38.6 mol % Cu-BTC with IL, (b) 20 mol % Cu-BTC with IL, (c) IL (EMIM-ETS), and (d) Cu-BTC.

observed in the vibrational spectra. For a sensible interpretation, the mutual interactions need to be considered.

Mutual Interactions between MOF and IL. Panels A and B in Figure 7 display the fingerprint regions of the FTIR and
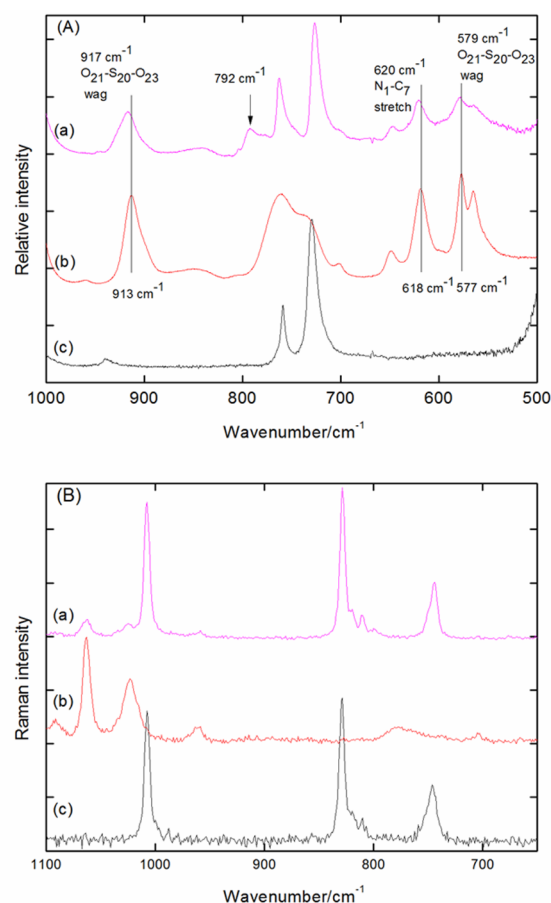

Figure 7. Experimental (A) FTIR and (B) Raman spectra: (a) 38.6 mol % Cu-BTC with IL, (b) IL (EMIM-ETS), and (c) Cu-BTC.

MOF leads to significant enhancement of the interionic interactions.

Other peaks in the vibrational spectra also reveal structural changes in the IL upon confinement. However, most of these changes are relatively small and should not be overinterpreted. For example, the 1 cm^{-1} frequency increase of the $C_{4,5}-H$ stretching mode of the imidazolium cation in the FTIR spectrum is virtually negligible. Small changes can also be observed in the 3000−2800 cm^{-1} range, where the aliphatic C−H stretches are detected. The dominating features in the Raman spectrum (Figure 6B) of the pure IL are the peaks at 2968 and 2943 cm^{-1}. In the MOF/IL sample, they shift to 2975 and 2937 cm^{-1}, respectively. The former can be assigned to C−H vibrations in the cationic alkyl chains, while the latter is likely to originate from the anion's ethyl moiety.

The anionic sulfate group is another moiety which will experience changes when the interionic interactions change. According to a previous study,[42] the S−O bond lengths for the lowest-energy ion-pair state in vacuo are 1.491 ($S-O_{21}$), 1.496 ($S-O_{22}$), 1.467 ($S-O_{23}$), and 1.666 Å ($S-O_{24}$), where O_{21} and O_{22} form hydrogen bonds with H_9, whereas O_{23} is not involved in the hydrogen bonding. Inside the MOF, they change significantly to 1.505 ($S-O_{21}$), 1.484 ($S-O_{22}$), 1.477 ($S-O_{23}$), and 1.634 Å ($S-O_{24}$), respectively. These changes cannot be correlated in a simple manner in terms of the phenomena

Raman spectra, respectively. The FTIR peaks at 577 and 913 cm^{-1} can be assigned to $O_{21}-S-O_{23}$ wagging and $O_{21}-S-O_{22}$ stretching vibrations, respectively. They show minor shifts to higher frequency upon confinement, which appears to be contradictory to the changes in the S−O bond lengths. To interpret the data correctly, the overall situation of the IL ion pair inside the MOF pore has to be taken into account. The simulation shows that the IL directly perturbs the whole structure and symmetry of Cu-BTC. The Cu ion is in the prominent site for interactions with the oxygen of the IL anion. Moreover, the computational data suggest that the IL preferentially interacts with those Cu ions, which are open and pointing into the larger pores. The presence of IL in these larger pores reduces the adsorption of water molecules at Cu ion sites and forces the water molecules into the smaller pores.[27] Therefore, the IL-induced changes in bond lengths and bond angles associated with Cu ions are different for large and small pores. The IL has also a direct effect on the MOF linker carboxylate (COO) and, to a smaller extent, on the benzene-ring-related C═C stretching vibrations. At the same time, MOF has also significant effect on the structure of IL following confinement. In general, two different types of IL ion-pair structure can be observed. The first one represents the ion pair

with an enhanced interionic interaction as described in the previous section. This was evidenced by the aforementioned reduction of the hydrogen bond distance between the cation and anion found in DFT simulations. The second ion-pair configuration exhibits a weakened interaction between the ions of IL. This species can be found in the presence of water molecules adsorbed in Cu-BTC. These water molecules are available to interact with ions of the IL, producing the weaker hydrogen bonding interactions between the cations and anions due to association with water molecules. The existence of both species is strongly supported by the experimental spectra. As discussed above, comparison of the C_2-H stretching mode of the pure IL and the confined IL shows one component that is slightly shifted to higher frequency (a few reciprocal centimeters) and one component that is strongly shifted to lower frequency (~ 20 cm^{-1}). In addition to these effects, it is also found that upon confinement of the IL in the MOF, the IL anion does not establish the only interactions with the MOF. The cationic imidazolium ring can interact in different ways with the anion and/or the MOF. The changes in interaction induced by confinement of the IL resulted in the reorganization of electron density. This can be analyzed via the difference electron density, which we consider next.

The DFT results for the difference electron density $\Delta\rho$ (= $\rho_{MOF+IL} - (\rho_{MOF} + \rho_{IL})$), i.e., electron density change arising from charge transfer and/or electron redistribution induced by the MOF–IL interactions, are exhibited in Figure 8 with $\Delta\rho$
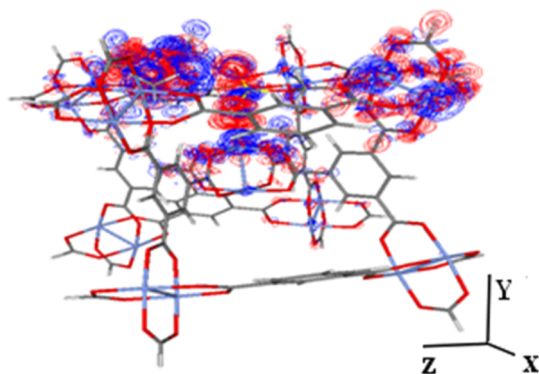

Figure 8. Difference electron density maps for the entire MOF + EMIM-ETS. The electron density redistribution induced by the MOF–IL interactions is shown in contours in the range between ±0.001 and ±0.0005 au. The blue and red contours represent regions of $\Delta\rho \leq 0$ and $\Delta\rho \geq 0$, respectively.

contours in the range of ±0.001 to ±0.0005 au displayed. The blue and red contours there denote $\Delta\rho < 0$ and $\Delta\rho > 0$, respectively. As expected, the electron density change in the MOF pore that directly interacts with the IL ion pair is much more pronounced than that in the opposite noninteracting pore. Though results presented here are based on interactions of a single ion pair with a model MOF system, it clearly shows that these interactions engender alterations of the electron density which can also gauge the conformation and structure changes within the MOF. While accurate quantification would require an increase in both the size of the model MOF system and the number of ion pairs in the DFT calculations, it is believed that the main qualitative and semiquantitative aspects of our results would remain valid.

For additional insight into charge transfer between the MOF and IL ion pair, the region of their direct interactions, is shown

enlarged in Figure 9. Both the Cu atom and the anion oxygen that interact with each other lose their electron density, which
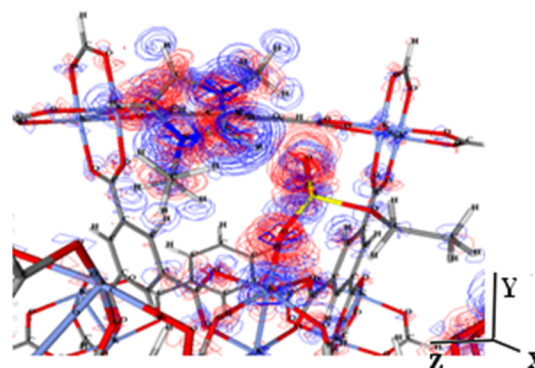

Figure 9. Difference electron density maps for charge-transfer region. As in Figure 8, $\Delta\rho$ contours in the range of ±0.001 to ±0.0005 au are displayed with $\Delta\rho \leq 0$ in blue and $\Delta\rho \geq 0$ in red.

is partly transferred along the interaction path and partly transferred to the anion's $S-O_{21}$ bond that interacts with the cation's H_9 at the C_2 position (Figure 2). As a result, the electron density of the $S-O_{21}$ bond becomes enhanced, making O_{21} relatively more electron-rich, as indicated by the presence of mainly red contours there. This electron density enhancement strengthens both the $S-O_{21}$ bond and the interionic $C_2-H_9\cdots O_{21}$ hydrogen bond, resulting in the reduction of their bond lengths, compared to the isolated ion pair. The depletion of electron density from H_9 (viz., blue contours there) is another indication of the enhanced $C_2-H_9\cdots O_{21}$ interaction. This was confirmed experimentally by the displacement of the band at 3084 cm^{-1} to lower frequency as discussed above. Thus, charge transfer or redistribution induced by the direct interaction of an anion with a MOF Cu atom leads to strengthening of the interaction of the same anion with a cation in the ionic liquid.

With this in mind, the experimental data can be placed in context. The FTIR peaks at 577 and 913 cm^{-1} can be assigned to $O_{21}-S-O_{23}$ wagging and $O_{21}-S-O_{22}$ stretching vibrations, respectively. Both modes show slight shifts toward higher frequency upon confinement, consonant with the $\Delta\rho$ analysis above, viz., the SO bonds interacting with the IL cation become strengthened because of their electron density enhancement engendered by the anion–MOF interactions.

Another particularly interesting feature in the FTIR spectrum is the appearance of an apparently new peak at 792 cm^{-1} when the IL is confined in the MOF. This peak may be the result of the formation of a new covalent bond between the IL and the Cu. Such a strong interaction is not predicted by the computational data. A closer look at the FTIR spectra in the range 800–700 cm^{-1} shows contributions from the MOF and the IL (Figure 7A). The MOF spectrum exhibits two distinct, slightly asymmetric peaks at 729 and 759 cm^{-1}, which can both be assigned to out-of-plane bending modes of the aromatic moieties of the linker (spectrum c in Figure 7A). The characteristic shapes of these two peaks can be easily identified in the spectrum of the IL/MOF sample (i.e., spectrum a) as well, and their center frequency is not significantly shifted. Hence, the new peak is unlikely to originate from the MOF. The pure IL spectrum (b in Figure 7A), on the other hand, exhibits a broad band centered at 761 cm^{-1} and having a shoulder at 734 cm^{-1}. Considering the band shapes, the new

peak at 792 cm^{-1} in the IL/MOF mixture and the 761 cm^{-1} peak in the pure IL may have the same origin. The 761 cm^{-1} peak of the IL can most likely be assigned to an S−O stretching vibration, which is significantly perturbed by the interaction with the MOF and thus shifted to 792 cm^{-1}. For completeness, it is noted that the 761 cm^{-1} peak was previously attributed to wagging of the cationic C$_4$−C$_5$−H moiety.[42] However, in light of the IL/MOF data, a reassignment to the S−O stretching vibration of the oxygen connecting the sulfate group with the ethyl chain (very strong) seems reasonable. The increase in the frequency of the reassigned mode upon confinement in the MOF can also be explained by the phenomena discussed above; hence, it lends further support to the interpretation.

■ CONCLUSIONS

The interactions of an imidazolium ionic liquid with Cu-BTC MOF were successfully investigated by experimental Raman and FTIR spectroscopies and density functional theory calculations. It was found that the confinement of the IL in the MOF perturbs the symmetry of the MOF. The interaction of the anion of the IL with metal Cu ions of the MOF leads to a significant enhancement of the interionic interactions. The DFT calculations and the Raman spectrum provide strong evidence for the anion−MOF interaction via a lengthening of the Cu−O bond and the corresponding decrease in the frequency of its vibrational mode, respectively. On the other hand, an increase in the frequency was found upon bond shortening of the Cu−O where the Cu ion of MOF is not involved in the interactions with the ETS anion. Consequently, our data suggest the presence of two different types of IL ion-pair configurations within the pores of the MOF: The first ion-pair configuration corresponds to an enhanced interionic interaction, and the second ion-pair configuration exhibits a weakened interaction between the ions of the IL. Apart from interactions of the anion of the IL with the Cu of MOF, the cation of the IL also interacts with either the anion or the MOF in different ways. The difference electron density analysis of DFT calculations also demonstrate that charge-transfer phenomenon or redistribution of electron density is responsible for the interaction between the MOF and IL. Additionally, the MESP isosurface indicates that adding further IL molecules can cause repulsion between the anion of the ionic liquid and the electronegative atom of the linkers in the MOF. This study on the confinement of ionic liquid in MOF will be useful for providing a platform to understand and enhance the behavior of IL-confined microporous systems as well as impact on host and guest and may reveal potential applications of this new type of "designer hybrid material" in energy storage systems.

■ AUTHOR INFORMATION

Corresponding Author
*E-mail: hjkim@cmu.edu.

Notes
The authors declare no competing financial interest.

■ ACKNOWLEDGMENTS

■ REFERENCES

(1) Chae, H. K.; Siberio-Pérez, D. Y.; Kim, J.; Go, Y.; Eddaoudi, M.; Matzger, A. J.; O'Keeffe, M.; Yaghi, O. M. A Route to High Surface Area, Porosity and Inclusion of Large Molecules in Crystals. *Nature* **2004**, *427*, 523−527.

(2) Li, J.; Kuppler, R. J.; Zhou, H. Selective Gas Adsorption and Separation in Metal-Organic Frameworks. *Chem. Soc. Rev.* **2009**, *38*, 1477−1504.

(3) Furukawa, H.; Ko, N.; Go, Y. B.; Aratani, N.; Choi, S. B.; Choi, E.; Yazaydin, A. O.; Snurr, R. Q.; O'Keeffe, M.; Kim, J.; et al. Ultrahigh Porosity in Metal-Organic Frameworks. *Science* **2010**, *329*, 424−428.

(4) Shekhah, O.; Liu, J.; Fischer, R.; Wöll, C. MOF Thin Films: Existing and Future Applications. *Chem. Soc. Rev.* **2011**, *40*, 1081−1106.

(5) Bohrman, J. A.; Carreon, M. A. Synthesis and CO$_2$/CH$_4$ Separation Performance of Bio-MOF-1 Membranes. *Chem. Commun.* **2012**, *48*, 5130−5132.

(6) Dalgarno, S. J.; Thallapally, P. K.; Barbour, L. J.; Atwood, J. L. Engineering Void Space in Organic Van Der Waals Crystals: Calixarenes Lead the Way. *Chem. Soc. Rev.* **2007**, *36*, 236−245.

(7) Nugent, P.; Belmabkhout, Y.; Burd, S. D.; Cairns, A. J.; Luebke, R.; Forrest, K.; Pham, T.; Ma, S.; Space, B.; Wojtas, L.; et al. Porous Materials with Optimal Adsorption Thermodynamics and Kinetics for CO$_2$ Separation. *Nature* **2013**, *495*, 80−84.

(8) Ramdin, M.; de Loos, T. W.; Vlugt, T. J. State-of-the-Art of CO$_2$ Capture with Ionic Liquids. *Ind. Eng. Chem. Res.* **2012**, *51*, 8149−8177.

(9) Welton, T. Room-Temperature Ionic Liquids. Solvents for Synthesis and Catalysis. *Chem. Rev.* **1999**, *99*, 2071−2084.

(10) Wasserscheid, P.; Keim, W. Ionic Liquids-New Solutions for Transition Metal Catalysis. *Angew. Chem., Int. Ed.* **2000**, *39*, 3772−3789.

(11) Seddon, K. R. Ionic Liquids for Clean Technology. *J. Chem. Technol. Biotechnol.* **1997**, *68*, 351−356.

(12) Hagiwara, R.; Ito, Y. Room Temperature Ionic Liquids of Alkylimidazolium Cations and Fluoroanions. *J. Fluorine Chem.* **2000**, *105*, 221−227.

(13) Huddleston, J. G.; Visser, A. E.; Reichert, W. M.; Willauer, H. D.; Broker, G. A.; Rogers, R. D. Characterization and Comparison of Hydrophilic and Hydrophobic Room Temperature Ionic Liquids Incorporating the Imidazolium Cation. *Green Chem.* **2001**, *3*, 156−164.

(14) Huddleston, J.; Willauer, H. D.; Swatloski, T. P.; Visser, A. E.; Rogers, R. D. Room Temperature Ionic Liquids as Novel Media for 'Clean'Liquid-Liquid Extraction. *Chem. Commun.* **1998**, 1765−1766.

(15) Cox, P. M.; Betts, R. A.; Jones, C. D.; Spall, S. A.; Totterdell, I. J. Erratum: Acceleration of Global Warming due to Carbon-Cycle Feedbacks in a Coupled Climate Model. *Nature* **2000**, *408*, 750−750.

(16) Babarao, R.; Dai, S.; Jiang, D. Understanding the High Solubility of CO$_2$ in an Ionic Liquid with the Tetracyanoborate Anion. *J. Phys. Chem. B* **2011**, *115*, 9789−9794.

(17) Yan, F.; Lartey, M.; Damodaran, K.; Albenze, E.; Thompson, R. L.; Kim, J.; Haranczyk, M.; Nulwala, H. B.; Luebke, D. R.; Smit, B. Understanding the Effect of Side Groups in Ionic Liquids on Carbon-Capture Properties: A Combined Experimental and Theoretical Effort. *Phys. Chem. Chem. Phys.* **2013**, *15*, 3264−3272.

(18) Kolding, H.; Fehrmann, R.; Riisager, A. CO$_2$ Capture Technologies: Current Status and New Directions using Supported Ionic Liquid Phase (SILP) Absorbers. *Sci. China: Chem.* **2012**, *55*, 1648−1656.

(19) Every, H. A.; Bishop, A. G.; MacFarlane, D. R.; Orädd, G.; Forsyth, M. Transport Properties in a Family of Dialkylimidazolium Ionic Liquids. *Phys. Chem. Chem. Phys.* **2004**, *6*, 1758−1765.

(20) Garcia, B.; Lavallée, S.; Perron, G.; Michot, C.; Armand, M. Room Temperature Molten Salts as Lithium Battery Electrolyte. *Electrochim. Acta* **2004**, *49*, 4583−4588.

(21) Kaar, J. L.; Jesionowski, A. M.; Berberich, J. A.; Moulton, R.; Russell, A. J. Impact of Ionic Liquid Physical Properties on Lipase Activity and Stability. *J. Am. Chem. Soc.* **2003**, *125*, 4125−4131.

(22) Cull, S.; Holbrey, J.; Vargas-Mora, V.; Seddon, K.; Lye, G. Room-temperature Ionic Liquids as Replacements for Organic Solvents in Multiphase Bioprocess Operations. *Biotechnol. Bioeng.* **2000**, *69*, 227−233.

(23) Singh, M. P.; Singh, R. K.; Chandra, S. Ionic Liquids Confined in Porous Matrices: Physicochemical Properties and Applications. *Prog. Mater. Sci.* **2014**, *64*, 73−120.

(24) Fujie, K.; Yamada, T.; Ikeda, R.; Kitagawa, H. Introduction of an Ionic Liquid into the Micropores of a Metal-Organic Framework and its Anomalous Phase Behavior. *Angew. Chem., Int. Ed.* **2014**, *53*, 11302−11305.

(25) Vicent-Luna, J. M.; Gutiérrez-Sevillano, J. J.; Anta, J. A.; Calero, S. Effect of Room-Temperature Ionic Liquids on CO_2 Separation by a Cu-BTC Metal-Organic Framework. *J. Phys. Chem. C* **2013**, *117*, 20762−20768.

(26) Chen, Y.; Hu, Z.; Gupta, K. M.; Jiang, J. Ionic Liquid/Metal-Organic Framework Composite for CO_2 Capture: A Computational Investigation. *J. Phys. Chem. C* **2011**, *115*, 21736−21742.

(27) Gutiérrez-Sevillano, J. J.; Vicent-Luna, J. M.; Dubbeldam, D.; Calero, S. Molecular Mechanisms for Adsorption in Cu-BTC Metal-Organic Framework. *J. Phys. Chem. C* **2013**, *117*, 11357−11366.

(28) Abroshan, H.; Kim, H. J. On the structural stability of ionic liquid-IRMOF composites: a computational study. *Phys. Chem. Chem. Phys.* **2015**, *17* (9), 6248−6254.

(29) Greathouse, J. A.; Allendorf, M. D. Force Field Validation for Molecular Dynamics Simulations of IRMOF-1 and Other Isoreticular Zinc Carboxylate Coordination Polymers. *J. Phys. Chem. C* **2008**, *112* (15), 5795−5802.

(30) Krishna, R.; van Baten, J. M. In Silico Screening of Metal-Organic Frameworks in Separation Applications. *Phys. Chem. Chem. Phys.* **2011**, *13*, 10593−10616.

(31) Amirjalayer, S.; Tafipolsky, M.; Schmid, R. Exploring Network Topologies of Copper Paddle Wheel Based Metal-Organic Frameworks with a First-Principles Derived Force Field. *J. Phys. Chem. C* **2011**, *115*, 15133−15139.

(32) Grajciar, L.; Bludský, O.; Nachtigall, P. Water Adsorption on Coordinatively Unsaturated Sites in Cu-BTC MOF. *J. Phys. Chem. Lett.* **2010**, *1*, 3354−3359.

(33) Fischer, M.; Hoffmann, F.; Fröba, M. New Microporous Materials for Acetylene Storage and C_2H_2/CO_2 Separation: Insights from Molecular Simulations. *ChemPhysChem* **2010**, *11*, 2220−2229.

(34) Wang, S.; Yang, Q.; Zhong, C. Adsorption and Separation of Binary Mixtures in a Metal-Organic Framework Cu-BTC: A Computational Study. *Sep. Purif. Technol.* **2008**, *60*, 30−35.

(35) Zhou, C.; Cao, L.; Wei, S.; Zhang, Q.; Chen, L. A First Principles Study of Gas Adsorption on Charged Cu-BTC. *Comput. Theor. Chem.* **2011**, *976*, 153−160.

(36) Greathouse, J. A.; Ockwig, N. W.; Criscenti, L. J.; Guilinger, T.; Pohl, P.; Allendorf, M. D. Computational Screening of Metal-Organic Frameworks for Large-Molecule Chemical Sensing. *Phys. Chem. Chem. Phys.* **2010**, *12*, 12621−12629.

(37) Bordiga, S.; Regli, L.; Bonino, F.; Groppo, E.; Lamberti, C.; Xiao, B.; Wheatley, P.; Morris, R.; Zecchina, A. Adsorption Properties of HKUST-1 Toward Hydrogen and Other Small Molecules Monitored by IR. *Phys. Chem. Chem. Phys.* **2007**, *9*, 2676−2685.

(38) Li, Y.; Yang, R. T. Hydrogen Storage in Metal-Organic Frameworks by Bridged Hydrogen Spillover. *J. Am. Chem. Soc.* **2006**, *128*, 8136−8137.

(39) Prestipino, C.; Regli, L.; Vitillo, J.; Bonino, F.; Damin, A.; Lamberti, C.; Zecchina, A.; Solari, P.; Kongshaug, K.; Bordiga, S. Local Structure of Framework Cu (II) in HKUST-1 Metallorganic Framework: Spectroscopic Characterization upon Activation and Interaction with Adsorbates. *Chem. Mater.* **2006**, *18*, 1337−1346.

(40) Küsgens, P.; Rose, M.; Senkovska, I.; Fröde, H.; Henschel, A.; Siegle, S.; Kaskel, S. Characterization of Metal-Organic Frameworks by Water Adsorption. *Microporous Mesoporous Mater.* **2009**, *120*, 325−330.

(41) Liang, Z.; Marshall, M.; Chaffee, A. L. Comparison of Cu-BTC and Zeolite 13X for Adsorbent Based CO_2 Separation. *Energy Procedia* **2009**, *1*, 1265−1271.

(42) Dhumal, N. R.; Kim, H. J.; Kiefer, J. Electronic Structure and Normal Vibrations of the 1-Ethyl-3-methylimidazolium Ethyl Sulfate Ion Pair. *J. Phys. Chem. A* **2011**, *115*, 3551−3558.

(43) Kelkar, M. S.; Shi, W.; Maginn, E. J. Determining the Accuracy of Classical Force Fields for Ionic Liquids: Atomistic Simulation of the Thermodynamic and Transport Properties of 1-Ethyl-3-methylimidazolium Ethyl Sulfate ($[Emim][EtSO_4]$) and its Mixtures with Water. *Ind. Eng. Chem. Res.* **2008**, *47*, 9115−9126.

(44) Malberg, F.; Pensado, A. S.; Kirchner, B. The Bulk and the Gas Phase of 1-Ethyl-3-Methyl imidazolium Ethyl Sulfate: Dispersion Interaction Makes the Difference. *Phys. Chem. Chem. Phys.* **2012**, *14*, 12079−12082.

(45) Kiefer, J.; Fries, J.; Leipertz, A. Experimental Vibrational Study of Imidazolium-Based Ionic Liquids: Raman and Infrared Spectra of 1-Ethyl-3-Methylimidazolium Bis (Trifluoromethylsulfonyl) Imide and 1-Ethyl-3-methylimidazolium Ethyl Sulfate. *Appl. Spectrosc.* **2007**, *61*, 1306−1311.

(46) Kiefer, J.; Molina, M. M.; Noack, K. The Peculiar Nature of Molecular Interactions between an Imidazolium Ionic Liquid and Acetone. *ChemPhysChem* **2012**, *13*, 1213−1220.

(47) Kiefer, J.; Namboodiri, M.; Kazemi, M. M.; Materny, A. Time-Resolved Femtosecond CARS of the Ionic Liquid 1-Ethyl-3-methylimidazolium Ethyl Sulfate. *J. Raman Spectrosc.* **2015**, *46*, 722−726.

(48) Noack, K.; Leipertz, A.; Kiefer, J. Molecular Interactions and Macroscopic Effects in Binary Mixtures of an Imidazolium Ionic Liquid with Water, Methanol, and Ethanol. *J. Mol. Struct.* **2012**, *1018*, 45−53.

(49) Becke, A. D. Density-functional Thermochemistry. III. the Role of Exact Exchange. *J. Chem. Phys.* **1993**, *98*, 5648−5652.

(50) Lee, C.; Yang, W.; Parr, R. G. Development of the Colle-Salvetti Correlation-Energy Formula into a Functional of the Electron Density. *Phys. Rev. B: Condens. Matter Mater. Phys.* **1988**, *37*, 785.

(51) Frisch, M.; et al. *Gaussian 09*, revision A.02; Gaussian. Inc.: Wallingford, CT, 2009.

(52) Gadre, S. R.; Bhadane, P. K.; Pundlik, S. S.; Pingale, S. S. In *Molecular Electrostatic Potentials: Concepts and Applications*; Murray, J. A., Sen, K, Eds.; Elsevier: Amsterdam, 1996; p 219.

(53) Limaye, A. C.; Gadre, S. R. UNIVIS-2000: An Indigenously Developed Comprehensive Visualization Package. *Curr. Sci. (India)* **2001**, *80*, 1296−1300.

(54) DeCoste, J. B.; Peterson, G. W.; Schindler, B. J.; Killops, K. L.; Browe, M. A.; Mahle, J. J. The Effect of Water Adsorption on the Structure of the Carboxylate Containing Metal-Organic Frameworks Cu-BTC, mg-MOF-74, and UiO-66. *J. Mater. Chem. A* **2013**, *1*, 11922−11932.

(55) Vairam, S.; Govindarajan, S. New Hydrazinium Salts of Benzene Tricarboxylic and Tetracarboxylic Acids—preparation and their Thermal Studies. *Thermochim. Acta* **2004**, *414*, 263−270.

(56) Petit, C.; Burress, J.; Bandosz, T. J. The Synthesis and Characterization of Copper-Based Metal-Organic Framework/Graphite Oxide Composites. *Carbon* **2011**, *49*, 563−572.